JOURNAL OF CATALYSIS **173,** 229–237 (1998)
ARTICLE NO. CA971911

NO Reduction with H_2 or CO over La_2O_3 and Sr-Promoted La_2O_3

S.-J. Huang, A. B. Walters, and M. A. Vannice

Department of Chemical Engineering, 107 Fenske Laboratory, Pennsylvania State University, University Park, Pennsylvania 16802-4400

Received August 8, 1997; revised September 23, 1997; accepted September 24, 1997

NO reduction with either H_2 or CO was studied between 773 and 973 K over La_2O_3 and Sr-promoted La_2O_3. In the absence of O_2 with H_2 as a reductant, the specific activity for NO disappearance (moles/s/m^2) over La_2O_3 at 773 K was 10-fold greater than that with CH_4, and at 973 K it was 19 times higher; however, the N_2/N_2O product ratio was only 0.27 at 773 K, although it increased to 1.4 at 973 K. With CO as the reductant and no O_2, specific activities were 4.4 and 6.5 times higher than with CH_4 at 773 and 973 K, respectively. In contrast to behavior with CH_4, the inclusion of 1% O_2 in the feed with H_2 or CO dramatically decreased activities because of direct combustion of the reductants. Specific activities were enhanced by the addition of 4% Sr to the La_2O_3 catalyst, particularly for N_2O formation. Adsorption of NO, O_2, CO, and H_2 was determined at 300 and 573 K, and substantial amounts of all but H_2 were adsorbed at the latter temperature. Based on sites counted by irreversible NO adsorption at 300 K, turnover frequencies on La_2O_3 for N_2 and N_2O formation with H_2 were 0.074 and 0.059 s^{-1} at 973 K, whereas the respective values with CO were 0.026 and 0.019 s^{-1}. A model is proposed for each reaction in the absence of O_2 that provides a rate expression that correlates very well with both the well-behaved Arrhenius plot for N_2 formation and the significant bend-over in N_2O formation as temperature increases.

INTRODUCTION

The catalytic reduction of NO_x to N_2, particularly in the presence of excess O_2, is an important environmental challenge. The current SCR technology uses NH_3; however, there are drawbacks with this process and the utilization of other reductants such as CH_4, CO, and H_2 would be desirable (1). During the past 3 years, rare earth oxides (REOs) and Sr-promoted REOs have been shown to be selective catalysts for NO reduction with CH_4 at temperatures above 800 K (2–5). It then became of interest to determine the behavior of these catalysts when H_2 or CO was used as the reductant, particularly in regard to lowering the operating temperature range and determining catalytic performance in the presence of excess O_2. Two of the best REO catalysts for the NO/CH_4 reaction were chosen—La_2O_3 and Sr-promoted La_2O_3—and NO reduction using either H_2 or CO as the reductant was examined over a range of temperatures and partial pressures to determine the kinetic behavior and to examine the effect of O_2 on these reactions. Although many studies of these two reactions on metal surfaces have been reported, studies involving nonmetallic catalysts are quite limited (6–11), and no pure REOs have been previously examined.

EXPERIMENTAL

The La_2O_3 samples were prepared by slurrying La_2O_3 (Rhone–Poulenc, 99.99%) in distilled, deionized water, drying overnight in an oven at 400 K, then calcining under flowing O_2 at 1023 K for 10 h. The 4% Sr/La_2O_3 sample was prepared by adding the appropriate amount of $Sr(NO_3)_2$ (Aldrich, 99.995%) to the slurry, drying in an oven overnight at 400 K, heating to 873 K for 1 h in a furnace to decompose $La(NO_3)_2$, then calcining at 1023 K for 10 h under flowing O_2. All samples were stored in a desiccator after calcination (12).

BET surface areas based on N_2 physisorption were measured in a Quantasorb system (Quantachrome Co.). Adsorption isotherms were obtained using a quartz cell attached to a system capable of a vacuum of 10^{-6} Torr at the sample (3). Constant temperature was attained with an Omega CN2011 temperature controller. All gases were UHP grade (MG Ind. or VWS, 99.999%) except for NO (MG Ind., 99.0%+). The standard pretreatment was that used before (2–5), i.e., heating at 973 K for 30 min under a flowing mixture of 10% O_2/90% He, evacuating at 973 K for 30 min, then cooling to the adsorption temperature. A 30-min evacuation at the adsorption temperature was conducted between the first and second isotherms.

The kinetic data were obtained in a reactor system described previously (13), typically under differential conditions. The gas mixtures used—4.04% NO/He, 3.84% NO/He, 3.83% H_2/He, 4.12% CO/He, and 9.9% O_2/He—were UHP (MG Ind., 99.999%) except for the NO (99.0%+). A gas chromatograph with 5A molecular sieve or Chromasorb 102 columns and the use of temperature programming gave quantitative separation for all products except NO_2 and H_2O. The standard pretreatment consisted of heating at 973 K for 1 h, after which time little CO_2 was detected. A period of 30 min on stream under each set of reaction

0021-9517/98 $25.00

conditions was allowed prior to effluent gas analysis, and data were gathered during ascending and descending temperature runs to check for deactivation. Arrhenius runs were conducted at 13 Torr NO with 13 Torr of either H_2 or CO, with He constituting the balance. During the partial pressure runs, the H_2 or CO pressure was held at 12.5 Torr while the NO pressure was varied from 3 to 13 Torr, and the NO pressure was held near 13 Torr while the H_2 or CO pressure was varied from 3 to 13 Torr.

RESULTS

Isotherms for NO and O_2 were measured at four temperatures from 300 to 773 K and have been shown elsewhere (14); CO and H_2 isotherms were measured at 300 and 573 K. Those for NO and CO at the two latter temperatures are shown in Fig. 1 and the uptakes for all four gases are given in Table 1. H_2 chemisorption was very low and no irreversible adsorption could be detected (12).

The reduction of NO using H_2 in the absence of gas-phase O_2 produced significant amounts of N_2O over both La_2O_3 and 4% Sr/La_2O_3 (Fig. 2). Trace amounts of NH_3 were sometimes observed. The high rates of N_2O formation contrast with those obtained using CH_4, which gave selectivities to N_2 of well over 90% (2, 5, 14). At 973 K, La_2O_3 showed substantial deactivation, whereas 4% Sr/La_2O_3 provided relatively stable activity maintenance (Fig. 3). The addition of 1% O_2 to the feed decreased the rate of NO reduction by an order of magnitude (Fig. 4). Under either set of reaction conditions used in Fig. 2 or Fig. 4, N_2 formation provided an extremely linear Arrhenius plot, whereas that for N_2O formation (and thus NO disappearance) revealed a pronounced curvature. In the absence of NO, H_2 combustion was also examined in an empty reactor as well as one containing either La_2O_3 or 4% Sr/La_2O_3, and the results are provided in Fig. 5.

Arrhenius plots for NO reduction with CO in the absence of O_2 are shown in Fig. 6 for La_2O_3 and 4% Sr/La_2O_3; comparable plots with 1% O_2 in the feed are provided in Fig. 7. Again, rates are quite high in the absence of O_2 and the addition of gas-phase oxygen decreases the NO conversion

TABLE 1

Adsorption of NO, O_2, H_2, and CO on La_2O_3 at 100 Torr

Adsorbate	Temperature (K)	Total uptake (μmole/g)	Irreversible uptake (μmole/m^2)	Total uptake (μmole/m^2)
NO	300	17.5[a]	5.6	7.2
	300	21.6	3.8	4.5
	573	25.9[b]	3.9	5.4
O_2	300	0.4[c]	0.07	0.13
	573	3.7[c]	0.4	1.1
H_2	300	0[d]	0	0
	573	0[d]	0	0
CO	300	4.3[d]	1.4	1.8
	573	3.4[d]	1.3	1.4

[a] 4% Sr/La_2O_3, surface area = 2.3 m^2/g.
[b] Surface area = 4.8 m^2/g.
[c] Surface area = 3.4 m^2/g.
[d] Surface area = 2.4 m^2/g.

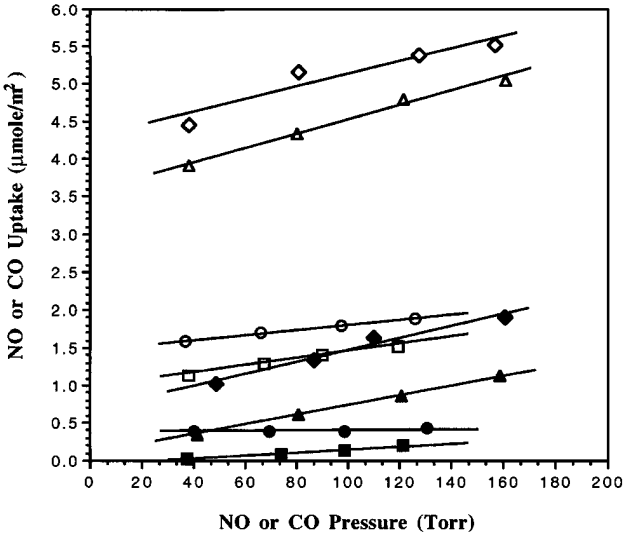

FIG. 1. NO and CO chemisorption on La_2O_3: 300 K—NO (▲, △), CO (●, ○); 573 K—NO (◆, ◇), CO (■, □); Total uptake (open symbols), reversible uptake (filled symbols).

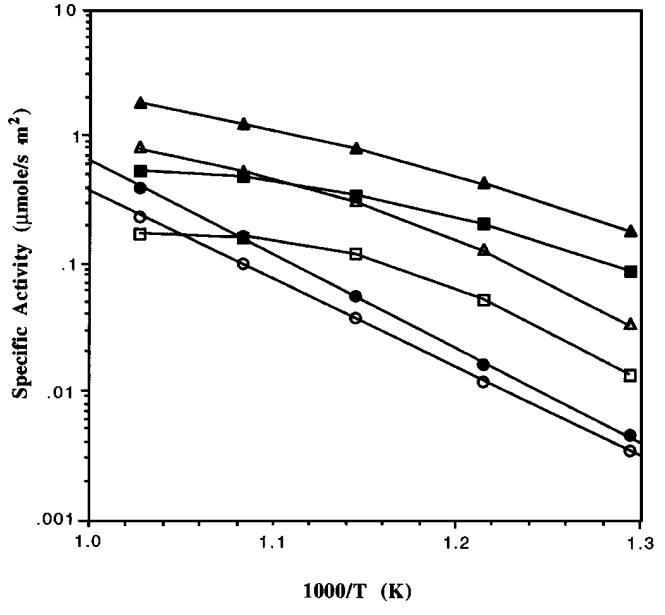

FIG. 2. NO reduction by H_2 over La_2O_3 (open symbols) and 4% Sr/La_2O_3 (filled symbols). Reaction conditions: 1 atm, 1.7% NO and 1.7% H_2 in He: (○, ●) N_2 formation, (□, ■) N_2O formation, (△, ▲) NO disappearance.

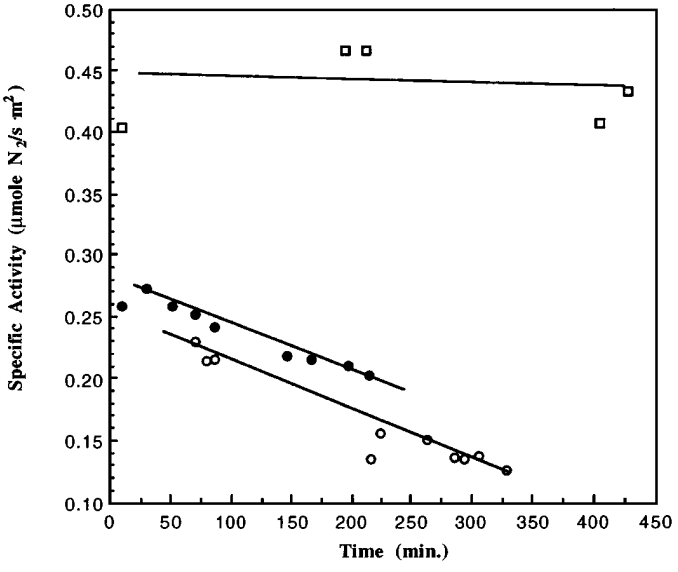

FIG. 3. Activity maintenance of La_2O_3 and Sr/La_2O_3 for the $NO + H_2$ reaction. Reaction conditions: 1 atm, 1.7% NO and 1.7% H_2 in He at 973 K: (□) 4% Sr/La_2O_3 (2.3 m^2/g), (●) La_2O_3 (3.4 m^2/g), (○) La_2O_3 (2.4 m^2/g).

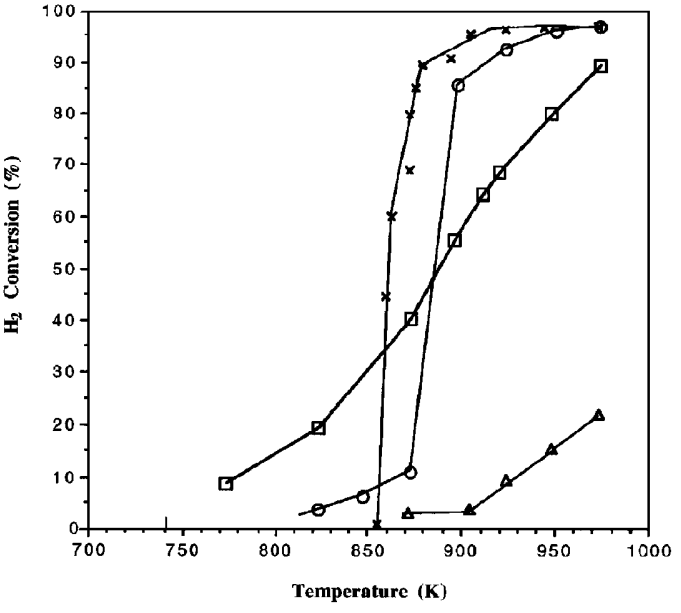

FIG. 5. H_2 combustion. Reaction conditions: 1 atm, 1.7% H_2, 1.0% O_2 in He (and 1.7% NO if co-fed): (○) $H_2 + O_2$ over La_2O_3, (□) $H_2 + O_2$ over 4% Sr/La_2O_3, (×) $H_2 + O_2$ in an empty reactor, (△) $H_2 + O_2 + NO$ in an empty reactor. The feed gas flow rate in the empty reactor was the same as that with La_2O_3.

rate, although not as severely as with H_2. Under either set of reaction conditions, N_2 formation gave extremely linear Arrhenius plots, whereas those for N_2O formation again showed significant curvature at higher temperatures. In all these runs, a GHSV of 77500 h^{-1} was used except for the run with 4% Sr/La_2O_3 using 1% O_2, when it was 38,800 h^{-1}. Table 2A lists the kinetic parameters for N_2 formation over these catalysts, and Table 2B gives the same information for N_2O. In the latter case, activation energies were evaluated using the linear portion of the Arrhenius plot below 873 K. The TOF values are based on adsorption sites counted by irreversible NO chemisorption at 300 K.

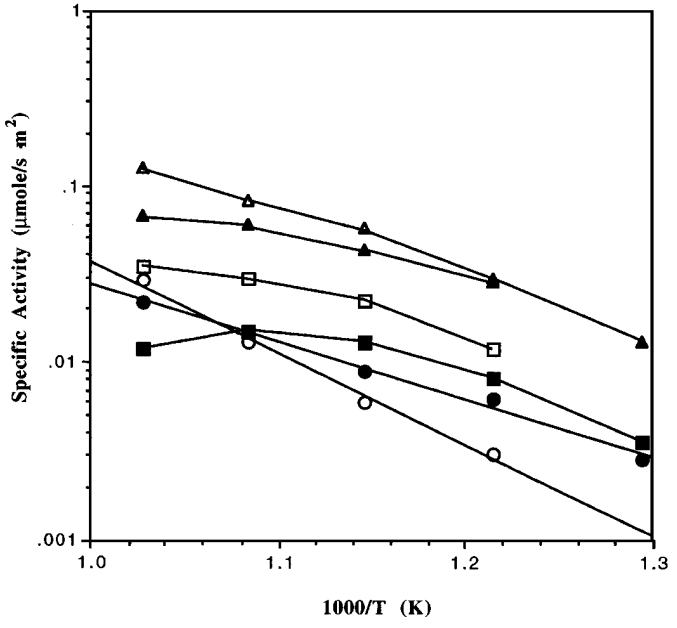

FIG. 4. NO reduction by H_2 (with O_2 present) over La_2O_3 (open symbols) and 4% Sr/La_2O_3 (filled symbols). Reaction conditions: 1 atm, 1.7% NO, 1.7% H_2 and 1.0% O_2 in He: (○, ●) N_2 formation, (□, ■) N_2O formation, (△, ▲) NO disappearance.

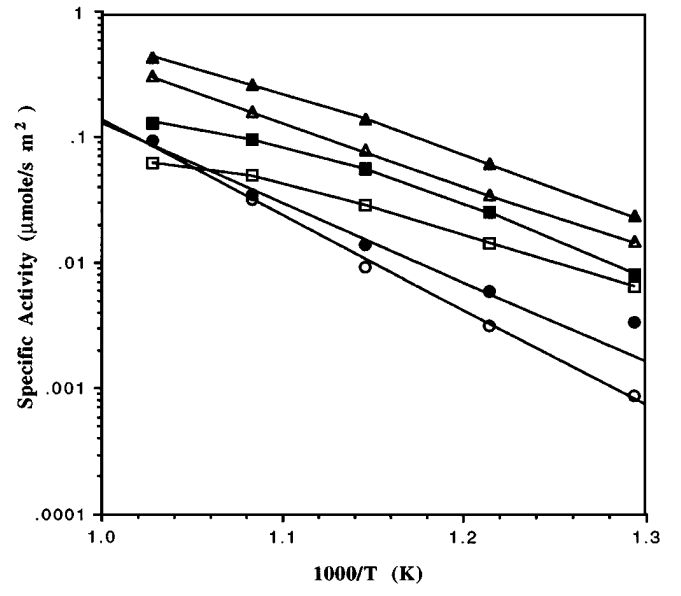

FIG. 6. NO reduction by CO over La_2O_3 (open symbols) and 4% Sr/La_2O_3 (filled symbols). Reaction conditions: 1 atm, 1.7% NO and 1.7% CO in He: (○, ●) N_2 formation, (□, ■) N_2O formation, (△, ▲) NO disappearance.

TABLE 2

NO Reduction by H_2 or CO over La_2O_3 and 4% Sr/La_2O_3[a] Reaction Cond.: $P = 1$ atm, 1.7% NO, 1.7% H_2 or CO, 1% O_2 when Present, Balance He

Catalyst	Reaction	E_a[b] (kcal/mole)	Rate (μmole N_2/s·g $\times 10^3$) 773 K	Rate (μmole N_2/s·g $\times 10^3$) 973 K	Specific activity (μmole N_2/s·m^2 $\times 10^3$) 773 K	Specific activity (μmole N_2/s·m^2 $\times 10^3$) 973 K	TOF ($s^{-1} \times 10^3$) 773 K	TOF ($s^{-1} \times 10^3$) 973 K	Selectivity[c] (%) 773 K	Selectivity[c] (%) 973 K
			A. N_2 formation							
La_2O_3	$NO + H_2$	31 ± 1	8.5	570	3.5	240	1.10	74	21	58
	$NO + H_2 + O_2$	24 ± 4	2.7	64	1.1	27	0.35	8.3	21	45
	$NO + CO$	35 ± 2	2.0	200	0.8	83	0.26	26	12	59
	$NO + CO + O_2$	33 ± 8	1.0	73	0.4	30	0.13	9.5	9	42
4% Sr/La_2O_3	$NO + H_2$	34 ± 1	10.2	911	4.4	400	0.72	64	5	41
	$NO + H_2 + O_2$	15 ± 2	7.6	55	3.3	24	0.54	3.9	45	65
	$NO + CO$	29 ± 5	4.1	194	1.8	84	0.29	14	18	41
	$NO + CO + O_2$	24 ± 3	3.5	49	1.5	21	0.25	3.4	19	51
	$NO + CH_4$	22 ± 5	8.7	175	3.8	76	0.61	12		>90
	$NO + CH_4 + O_2$	26 ± 5	18.5	603	8.0	262	1.30	43		>90
			B. N_2O formation							
La_2O_3	$NO + H_2$	29	33	406	14	170	4.2	59		
	$NO + H_2 + O_2$	27	7.4	84	3.1	35	1.0	11		
	$NO + CO$	20	16	148	6.6	62	2.1	19		
	$NO + CO + O_2$	32	9.8	103	4.1	43	1.3	13		
4% Sr/La_2O_3	$NO + H_2$	18	206	1230	90	535	14.5	87		
	$NO + H_2 + O_2$	17	8.9	30	3.9	13	0.6	2.1		
	$NO + CO$	26	19	302	8.3	131	1.3	21		
	$NO + CO + O_2$	27	14	47	6.2	20	1.0	3.3		

[a] Reaction conditions: $P = 1$ atm, 17% NO, 1.7% H_2 or CO, 1% O_2 when present, balance He.
[b] Evaluated with 90% confidence limits.
[c] S = moles N_2/(moles N_2 + moles N_2O).
[d] From Ref. (14).
[e] Evaluated below 873 K.

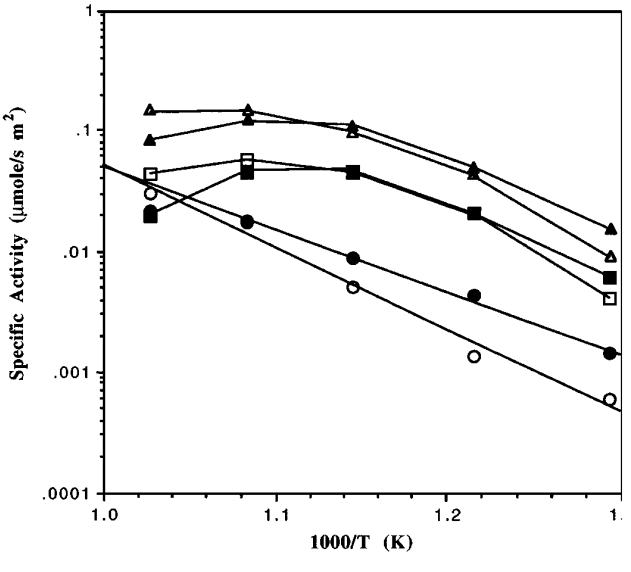

FIG. 7. NO reduction by CO (with O_2 present) over La_2O_3 (open symbols) and 4% Sr/La_2O (filled symbols). Reaction conditions: 1 atm, 1.7% NO, 1.7% CO, and 1.0% O_2 in He: (○, ●) N_2 formation, (□, ■) N_2O formation, (△, ▲) NO disappearance.

The maximum H_2 conversion in the $NO + H_2$ runs was 26%, whereas in the $NO + CO$ runs maximum CO conversion was 7%. In the $NO + H_2 + O_2$ and $NO + CO + O_2$ runs, the highest H_2 or CO conversions ranged from 46 to 58%, except for the experiment with 4% Sr/La_2O_3 at lower SV when H_2 conversion reached 96%. Thus, with exception of this last run, ample H_2 or CO remained at the bed exit for reaction with NO, and the bend-over observed for N_2O cannot be attributed to extremely low reactant concentrations caused by combustion.

The partial pressure dependencies for the $NO + H_2$ reaction were determined at 823, 848, and 873 K, and reaction orders obtained from a fit to a power rate law are listed in Table 3. Higher temperatures of 873, 893, and 913 K were used for determining partial pressure dependencies for the $NO + CO$ reaction, and these reaction orders are given in Table 4. The data points provided later in Fig. 9 show the fit of the reaction models to the measured rates.

DISCUSSION

Most studies of the $NO + H_2$ reaction have involved metals as catalysts, and only four papers were found dealing with this reaction over nonmetallic catalysts. Iizuka *et al.*

TABLE 3

Partial Pressure Dependencies for the NO + H_2 Reaction over La_2O_3

	Reaction temperature (K)	Reaction order in NO[a]	Reaction order in H_2[b]
NO disappearance	823	0.41	0.59
	848	0.47	0.67
	873	0.54	0.66
N_2 formation	823	0.27	0.65
	848	0.28	0.53
	873	0.40	0.67
N_2O formation	823	0.45	0.58
	848	0.53	0.71
	873	0.60	0.66

[a] $P_{H_2} = 12.5$ Torr.
[b] $P_{NO} = 13.1$ Torr.

used Fe_2O_3 dispersed on various oxides as a catalyst (6), Shelef and Gandhi investigated numerous oxides including those of Cu, Cr, Fe, and Ni (7), Mochida *et al.* reported on the behavior of Co tetraphenylporphyrin supported on TiO_2 (8), and Lindstedt *et al.* examined $La_{1-x}Sr_xMO_3$ perovskites (M is a transition metal) as catalysts for both this reaction and the NO + CO reaction (9). Mizuno *et al.* also studied the latter reaction over this same family of perovskite catalysts (10). The limited earlier work on the NO + CO reaction has been reviewed by Viswanathan (11). Pure REOs have not been investigated for either reaction.

The uptake results in Table 1 establish that NO has the largest adsorption capacity on La_2O_3 at 300 K followed by CO. Oxygen adsorption is much lower at 300 K compared with 573 K, while no significant hydrogen adsorption occurs at either temperature. The surface coverage by NO is substantial and represents about 10% of the surface even if no dissociation occurs. Although current TPD studies have shown that three different NO desorption peaks are observed, the exact nature of these sites is still under study and is not yet known (15). Earlier studies have reported that CO chemisorption on some REOs such as Nd_2O_3, CeO_2, and Er_2O_3 occurs only at higher temperatures (16); however, this is probably dependent on pretreatment. This same reference has reported that two forms of adsorbed hydrogen can exist on REOs: a weakly bound species desorbing around 253 K and a more strongly bound species desorbing near 473 K, with only the former species occurring on La_2O_3 (18). Our results are consistent with this report.

The investigation of H_2 combustion showed that almost no reaction occurred on La_2O_3 at 773 K and only about 10% of the H_2 was converted at 873 K; then a dramatic increase in rate took place during the next 25 K, as shown in Fig. 5. This is almost certainly due to the homogeneous gas-phase reaction which becomes significant above 860 K, as indicated in the same figure. Although H_2 conversion on the 4% Sr/La_2O_3 catalyst was higher at 773 K, the increase in rate with temperature appeared always to be dominated by the heterogeneous reaction. The addition of NO to the feed markedly suppressed the homogeneous $H_2 + O_2$ reaction, and the total conversion of H_2 at 973 K was less than 25% (Fig. 5). This suppression of homogeneous gas-phase H_2 combustion in the presence of NO would imply that heterogeneously catalyzed reactions should dominate under our experimental conditions.

At 773 K in the absence of O_2, H_2 reacts readily with NO and the specific activity for NO reduction by H_2 is similar to but higher than that with CH_4, as illustrated for the 4% Sr/La_2O_3 catalyst in Table 2, and at 973 K the activity is much higher than that with CH_4, even with O_2 present. The addition of O_2 to the feedstream clearly decreases the reaction between NO and H_2, but enhances that involving CH_4 and NO, as known previously (2–5); the relative reduction in rate becomes more severe as the temperature increases. The activation energy for the NO + H_2 reaction is substantially higher than that for the NO + CH_4 reaction, but in the presence of O_2 it is markedly decreased; in contrast, it becomes larger when CH_4 is involved. In contrast with the use of CH_4, N_2O formation is very significant, and the high selectivities to N_2O are clearly evident at 773 K; however, they decrease significantly at 973 K to give comparable amounts of N_2 and N_2O. As also demonstrated in Table 2, the specific activities for NO reduction with CO are clearly lower at 773 K in the absence of O_2 than those with H_2 and CH_4, but the addition of O_2 to the feed does not reduce the rate as severely as with H_2. Furthermore, the effect of O_2 on the activation energy is much smaller. The selectivity to N_2O at 773 K is very high when CO is

TABLE 4

Partial Pressure Dependencies for the NO + CO Reaction over La_2O_3

	Reaction temperature (K)	Reaction order in NO[a]	Reaction order in CO[b]
NO disappearance	873	0.55	0.53
	893	0.52	0.60
	913	0.57	0.59
N_2 formation	873	0.31	0.60
	893	0.45	0.70
	913	0.56	0.80
N_2O formation	873	0.66	0.50
	893	0.56	0.60
	913	0.57	0.48

[a] $P_{CO} = 12.5$ Torr.
[b] $P_{NO} = 12.5$ Torr.

used, although it begins to approach one-half at 973 K. In all cases it appears that N_2O is a primary product when H_2 or CO is used.

Previous studies with which these results can be compared are very limited. Over their family of perovskites, Lindstedt *et al.* investigated the $NO + H_2$ reaction (1000 ppm NO, 2000 ppm H_2) and the $NO + CO$ reaction (1000 ppm NO, 1% CO) between 873 and 1223 K, and they found CO was the better reductant (9). The addition of 4% O_2 to the second reaction resulted in no NO reduction, and in some cases the perovskites decomposed to give La_2O_3 and the metal. No specific activities were reported or could be calculated. The only study reporting specific activities was that of Mizuno *et al.* for the $NO + CO$ reaction over the same family of perovskites; for comparison, at 573 K and 30 Torr each of NO and CO, the most active catalyst, $LaCoO_3$, and the least active catalyst, $LaNiO_3$, gave specific activities of 0.52 and 0.017 μmole CO/s/m^2 (10). After the results for La_2O_3 in Table 2 are converted to CO consumption, the specific activity at 773 K is then 0.0082 μmole CO/s/m^2; thus this REO is much less active than the perovskites although the N_2O/N_2 selectivities are similar.

Based on the observation that N_2O is a primary product coupled with the significant curvature of the N_2O Arrhenius plots, an effort was made to propose a reaction model that could not only explain this behavior, but also fit the partial pressure dependencies that were obtained at three temperatures. More than 20 models were tested for H_2 and discarded. These mechanisms included (1) use of an irreversible N_2O* formation step with either one or two types of sites, (2) the formation of $NHO*$ as a quasi-equilibrated step, (3) the assumption of either $H*$ or $O*$ as one of the most abundant surface intermediates, (4) N_2O* decomposition as a single rate-determining step, (5) reaction between $NO*$ and $OH*$ to form $NHO*$ and $O*$ as a slow step, (6) the assumption of nondissociative H_2 adsorption, and (7) the formation of N_2O* and $O*$ from $2NO*$ as the rate-determining step with the role of hydrogen being only to remove $O*$ via H_2O. These models were rejected because either they did not fit the data satisfactorily or they provided fitting parameters giving physically meaningless thermodynamic values (12). Only two models were found that could provide a satisfactory fit, and the preferred one is illustrated here by the sequence of elementary steps shown below for the $NO + H_2$ reaction:

$$2\left[\mathrm{NO} + * \overset{K_{\mathrm{NO}}}{\rightleftharpoons} \mathrm{NO}*\right], \quad [1]$$

$$2\left[\mathrm{H_2} + 2\mathrm{S} \overset{K_{\mathrm{H_2}}}{\rightleftharpoons} 2\mathrm{H{-}S}\right], \quad [2]$$

$$\mathrm{NO}* + \mathrm{H{-}S} \overset{k_0}{\rightarrow} \mathrm{HNO}* + \mathrm{S}, \quad [3]$$

$$\mathrm{HNO}* + \mathrm{NO}* \overset{k_1}{\rightarrow} \mathrm{N_2O}* + \mathrm{OH}*, \quad [4]$$

$$\mathrm{N_2O}* \overset{k_2}{\rightarrow} \mathrm{N_2(g)} + \mathrm{O}*, \quad [5]$$

$$\mathrm{N_2O}* \underset{k_{-3}}{\overset{k_3}{\rightleftharpoons}} \mathrm{N_2O(g)} + *, \quad [6]$$

$$\mathrm{OH}* + \mathrm{H{-}S} \overset{K_4}{\rightleftharpoons} \mathrm{H_2O(g)} + * + \mathrm{S}, \quad [7]$$

$$2\mathrm{H{-}S} + \mathrm{O}* \overset{K_5}{\rightleftharpoons} \mathrm{H_2O(g)} + * + 2\mathrm{S}. \quad [8]$$

The adsorption steps for the two reactants are assumed to be in quasi-equilibrium. N_2O is formed on the surface by an irreversible step, as is N_2, and a reversible adsorption/desorption step for NO is proposed to allow gas-phase N_2O to occur. Two different types of sites, $*$ and S, are used to be consistent with the markedly different chemisorption uptake results for NO and H_2 in Table 1; however, this assumption is not required and a one-site sequence can also give a satisfactory fit (12). Steps [3]–[5], [7], and [8] have their counterparts in known homogeneous, free-radical reactions (17). Note that k_1 incorporates a (z/L_*) term needed to represent pairs of $*$ sites, where Z is a local coordination number (18).

In the absence of gas-phase O_2, the rates of NO disappearance, N_2 formation, and net N_2O production can be written respectively as

$$r_{\mathrm{NO}} = -dn_{\mathrm{NO}}/dt = 2r_{(3)} = 2L_*L_{\mathrm{S}}k_0\theta_{\mathrm{NO}}\theta_{\mathrm{H}}, \quad [9]$$

$$r_{\mathrm{N_2}} = dn_{\mathrm{N_2}}/dt = r_{(5)} = L_*k_2\theta_{\mathrm{N_2O}}, \quad [10]$$

$$r_{\mathrm{N_2O}} = dn_{\mathrm{N_2O}}/dt = r_{(6)} = L_*k_3\theta_{\mathrm{N_2O}} - L_*k_{-3}P_{\mathrm{N_2O}}\theta_{\mathrm{V}*}, \quad [11]$$

where L_* and L_{S} represent the total numbers of $*$ and S sites per square meter, respectively, and V_* represents vacant $*$ sites. From steps [1] and [2],

$$\theta_{\mathrm{NO}} = K_{\mathrm{NO}}P_{\mathrm{NO}}\theta_{\mathrm{V}*}, \quad [12]$$

$$\theta_{\mathrm{H}} = K_{\mathrm{H_2}}^{1/2}P_{\mathrm{H_2}}^{1/2}\theta_{\mathrm{V}}. \quad [13]$$

Using the steady-state approximation, balances on $HNO*$ and N_2O* species give

$$d[\mathrm{HNO}*]/dt = 0 = L_*L_{\mathrm{S}}k_0\theta_{\mathrm{NO}}\theta_{\mathrm{H}} - L_*k_1\theta_{\mathrm{HNO}}\theta_{\mathrm{NO}}, \quad [14]$$

$$d[\mathrm{N_2O}*]/dt = 0 = L_*k_1\theta_{\mathrm{HNO}}\theta_{\mathrm{NO}} + L_*k_{-3}P_{\mathrm{N_2O}}\theta_{\mathrm{V}*} - L_*k_2\theta_{\mathrm{N_2O}} - L_*k_3\theta_{\mathrm{N_2O}}. \quad [15]$$

Assuming that $NO*$ is the most abundant surface intermediate on the $*$ sites gives $L_* = [*] + [\mathrm{NO}*]$. The influence of H_2O is not included because the rate data were obtained under differential reaction conditions. Making the appropriate substitutions and further assuming that the coverage by H atoms is very low, i.e., $[\mathrm{HS}] \ll [\mathrm{S}]$, then the rate equations below are obtained, where $k_2' = L_*k_2$, $k_3' = L_*k_3$, and

$k'_{-3} = L_* k_{-3}$, respectively:

$$r_{NO} = \frac{2L_* L_S k_0 K_{NO} K_{H_2}^{1/2} P_{NO} P_{H_2}^{1/2}}{1 + K_{NO} P_{NO}} = \frac{k P_{NO} P_{H_2}^{1/2}}{1 + K_{NO} P_{NO}}, \quad [16]$$

$$r_{N_2} = L_* k_2 \left[\frac{L_S k_0 K_{NO} K_{H_2}^{1/2} P_{NO} P_{H_2}^{1/2} + k_{-3} P_{N_2O}}{(k_2 + k_3)(1 + K_{NO} P_{NO})} \right]$$

$$= \frac{0.5 k'_2 k P_{NO} P_{H_2}^{1/2} + k'_2 k'_{-3} P_{N_2O}}{(k'_2 + k'_3)(1 + K_{NO} P_{NO})}, \quad [17]$$

$$r_{N_2O} = L_* k_3 \left[\frac{L_S k_0 K_{NO} K_{H_2}^{1/2} P_{NO} P_{H_2}^{1/2} + k_{-3} P_{N_2O}}{(k_2 + k_3)(1 + K_{NO} P_{NO})} \right]$$

$$- \left[\frac{L_* k_{-3} P_{N_2O}}{1 + K_{NO} P_{NO}} \right] = \frac{0.5 k'_3 k P_{NO} P_{H_2}^{1/2} - k'_2 k'_{-3} P_{N_2O}}{(k'_2 + k'_3)(1 + K_{NO} P_{NO})}. \quad [18]$$

The mass balance equations for a fixed bed reactor can now be employed:

$$-dF_{NO}/dW = r_{NO}, \quad [19]$$

$$-dF_{H_2}/dW = -0.5 r_{NO}, \quad [20]$$

$$-dF_{N_2}/dW = r_{N_2}, \quad [21]$$

$$-dF_{N_2O}/dW = r_{N_2O}. \quad [22]$$

Here F_i is given in micromoles per second and W is catalyst weight in grams. Solving these four differential equations simultaneously using known initial conditions gives the concentration profile for each species through the catalyst bed; however, with H_2 five parameters must be known, i.e., k, K_{NO}, k'_2, k'_3, and k'_{-3}, thus some additional information must be used to obtain values for all parameters and to calculate rates quantitatively. The k values can be obtained directly by substituting Eq. [16] into Eq. [19], integrating it, and fitting it to the experimental data in Fig. 2. The $K_{NO} = e^{\Delta S^0_{ad}/R} e^{-\Delta H^0_{ad}/RT}$ values were forced to be physically meaningful by using an enthalpy of adsorption of $\Delta H^0_{ad} = -28$ kcal/mole and an entropy of adsorption of $\Delta S^0_{ad} = -23$ cal/mole/K obtained in a study of NO reduction by CH_4 over this same La_2O_3 catalyst at three temperatures (12, 14). A somewhat better fit was obtained if K_{NO} were used as a completely adjustable parameter, but the enthalpy and entropy values were not so consistent. A relationship between k'_3 and k'_{-3} can be provided if the equilibrium adsorption constant for K_{N_2O} is known, i.e., $k'_{-3}/k'_3 = K_{N_2O}$, and if N_2O adsorption is nonactivated, then $E_{desorption} = E_3 = -\Delta H^0_{ad}$. No K_{N_2O} values for La_2O_3 have been reported; however, these values were estimated using $\Delta H^0_{ad} = -13$ kcal/mole and $\Delta S^0_{ad} = -20$ cal/mole/K, which are average values for N_2O adsorption on Mn_2O_3 based on our recent study of N_2O decomposition (19) and an earlier study of this same reaction by Rheaume and Parravano (20). The ΔS^0_{ad} value is obtained from a previously reported correlation between ΔS^0_{ad} and ΔH^0_{ad} (21, 22). Consequently, only k'_2 and k'_3 remain as fitting parameters and these values were obtained by optimizing the fit to the data for N_2 and N_2O formation, as shown in Fig. 8a, as well as the pressure dependencies depicted

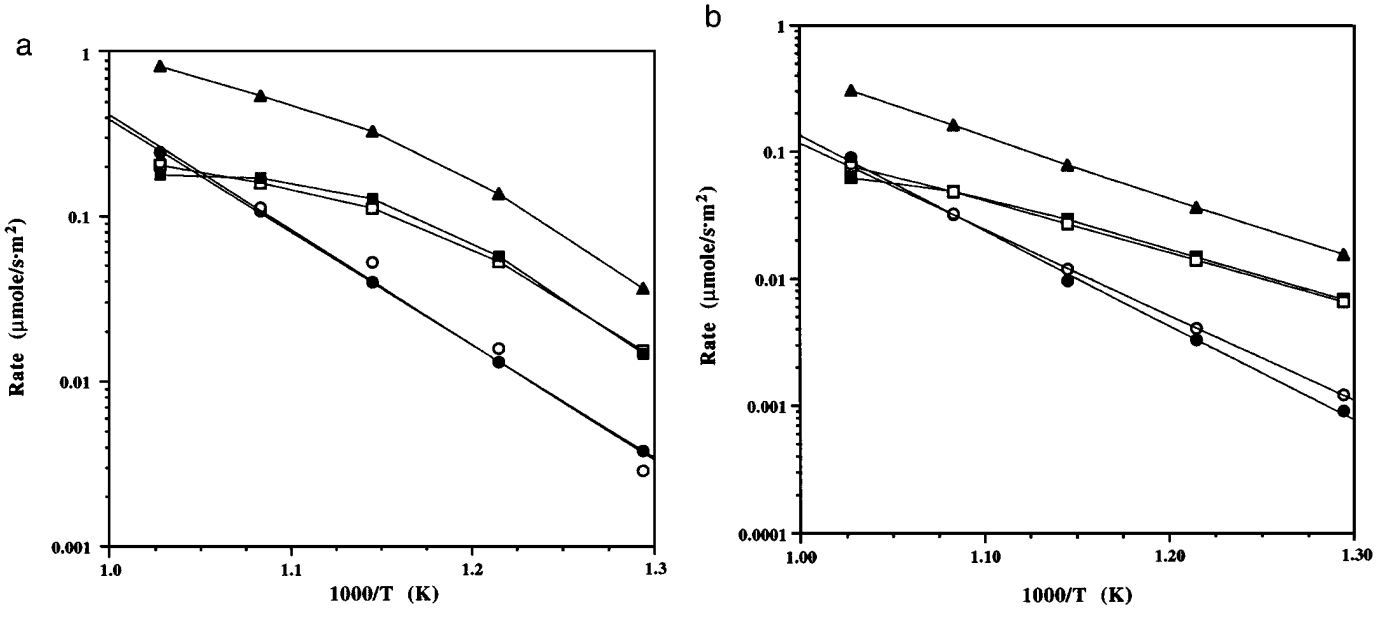

FIG. 8. (a) Comparison of reaction model with data for the $NO + H_2$ reaction over La_2O_3 in the absence of O_2 using Eqs. [16]–[18] and parameter values in Table 5. (b) Comparison of reaction model with data for the $NO + CO$ reaction over La_2O_3 in the absence of O_2 using Eqs. [30]–[32] and parameter values in Table 5. Open symbols: from model; filled symbols: experimental data. (△, ▲) r_{NO}, (□, ■) r_{N_2O}, (○, ●) r_{N_2}.

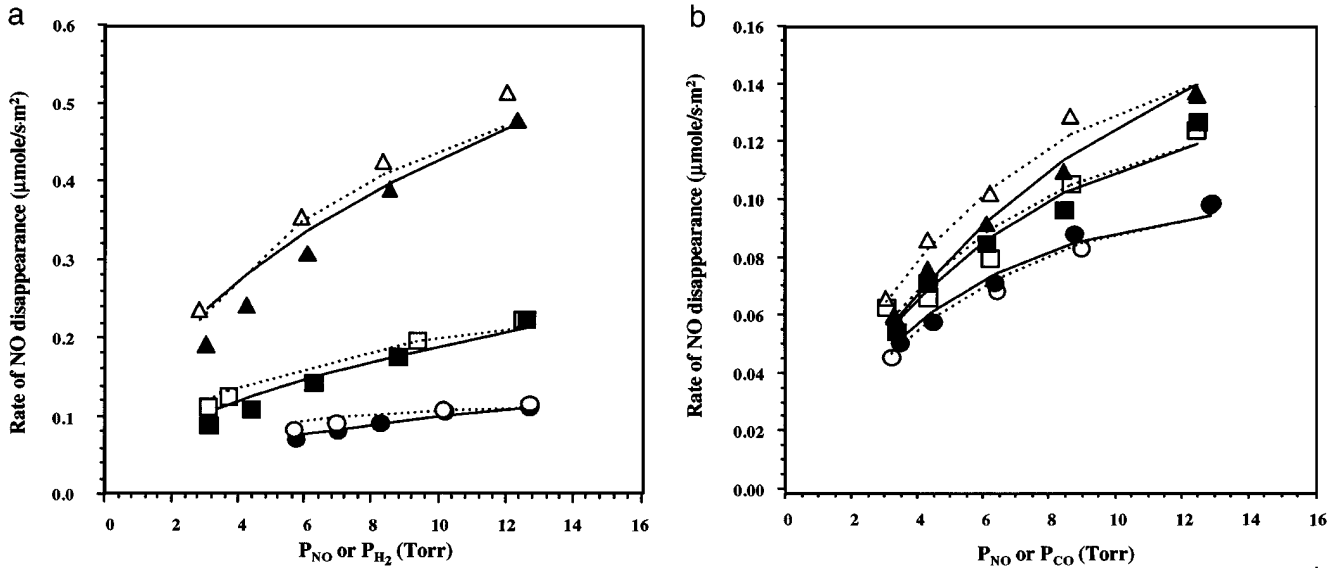

FIG. 9. (a) Fit of reaction model for the $NO + H_2$ reaction over La_2O_3 to pressure dependency data using Eq. [16] and parameter values in Table 5. Open symbols and dotted lines: NO pressure; filled symbols and solid lines: H_2 pressure. (○, ●) 823 K, (□, ■) 848 K, (△, ▲) 873 K. (b) Fit of reaction model for the $NO + CO$ reaction over La_2O_3 to pressure dependency data using Eq. [30] and parameter values in Table 5. Open symbols and dotted lines: NO pressure; filled symbols and solid lines: CO pressure. (○, ●) 873 K, (□, ■) 893 K, (△, ▲) 913 K.

in Fig. 9a. Since surface areas are known, rates have been converted to specific activities. The fit shown was obtained with $k_2' = 1.1 \times 10^9 e^{-24{,}000/RT}$ and $k_3' = 5 \times 10^6 e^{-13{,}000/RT}$ μmole/s/m^2. With these constraints on the fitting parameters, good agreement was obtained for all the results in these two figures. Rather than a precise fit of all data, the most important aspect of this exercise is the verification that the pronounced bend-over in N_2O formation at high temperatures can be adequately modeled by including a reversible adsorption/desorption step for N_2O. The values of the various parameters at five temperatures are listed in Table 5.

A similar approach to obtain a reaction model can be used for the $NO + CO$ reaction in the absence of gas-phase O_2, but with one small difference based on the more comparable uptakes of NO and CO listed in Table 1; i.e., CO is assumed to adsorb on the same sites as NO. This assumption is also supported by recent TPD results showing that preadsorbed CO inhibits NO chemisorption (15). The sequence is then

$$2\left[\mathrm{NO} + * \overset{K_{\mathrm{NO}}}{\rightleftharpoons} \mathrm{NO}*\right], \quad [23]$$

$$2\left[\mathrm{CO} + * \overset{K_{\mathrm{CO}}}{\rightleftharpoons} \mathrm{CO}*\right], \quad [24]$$

$$\mathrm{NO}* + \mathrm{CO}* \overset{k_0}{\rightarrow} \mathrm{NCO}* + \mathrm{O}*, \quad [25]$$

$$\mathrm{NCO}* + \mathrm{NO}* \overset{k_1}{\rightarrow} \mathrm{N_2O}* + \mathrm{CO}*, \quad [26]$$

$$\mathrm{N_2O}* \overset{k_2}{\rightarrow} \mathrm{N_2} + \mathrm{O}*, \quad [27]$$

$$\mathrm{N_2O}* \underset{k_{-3}}{\overset{k_3}{\rightleftharpoons}} \mathrm{N_2O} + *, \quad [28]$$

$$2\left[\mathrm{CO}* + \mathrm{O}* \overset{K_4}{\rightleftharpoons} \mathrm{CO_2} + 2*\right]. \quad [29]$$

These steps again have their gas-phase, free radical counterparts (18). If [NO∗] and [CO∗] are assumed to be the

TABLE 5

Parameter Values Used to Optimize Eqs. [16]–[18] for the $NO + H_2$ Reaction and Eqs. [30]–[32] for the $NO + CO$ Reaction on La_2O_3

T (K)	$k(NO + H_2)$ (μmole/s · m^2 · atm$^{3/2}$)	$k(NO + CO)$ (μmole/s · m^2 · atm^2)	k_2' (μmole/s · m^2)	k_3' (μmole/s · m^2)	K_{NO} (atm^{-1})	K_{N_2O} (atm^{-1})	K_{CO} (atm^{-1})
773	279	207000	195	587	942	0.20	2770
823	393	28900	498	1760	312	0.12	532
873	463	6980	1150	2780	114	0.076	122
923	489	3370	2410	4170	49	0.051	34
973	594	2650	4710	6010	22	0.035	11

predominant surface species, then rate equations for NO consumption, N_2 formation, and N_2O production can be obtained in the same manner as before (12):

$$r_{NO} = \frac{k P_{NO} P_{CO}}{(1 + K_{NO} P_{NO} + K_{CO} P_{CO})^2}, \quad [30]$$

$$r_{N_2} = \frac{k k'_2 P_{NO} P_{CO} + k'_2 k'_{-3} (1 + K_{NO} P_{NO} + K_{CO} P_{CO}) P_{N_2O}}{(k'_2 + k'_3)(1 + K_{NO} P_{NO} + K_{CO} P_{CO})^2}, \quad [31]$$

$$r_{N_2O} = \frac{k k'_3 P_{NO} P_{CO} - k'_2 k'_{-3} (1 + K_{NO} P_{NO} + K_{CO} P_{CO}) P_{N_2O}}{(k'_2 + k'_3)(1 + K_{NO} P_{NO} + K_{CO} P_{CO})^2}. \quad [32]$$

The influence of CO_2 is not included because the rate data were obtained under differential reaction conditions. The values of the same five parameters—k, K_{NO}, k'_2, k'_3, and k'_{-3}—were obtained exactly as before while values for the extra fitting parameter, K_{CO}, were acquired by optimizing the fits with the CO pressure dependencies at 873, 893, and 913 K, which are provided in Fig. 9b. This gave values of $\Delta H^0_{ad} = -41$ kcal/mole and $\Delta S^0_{ad} = -38$ cal/mole/K for CO adsorption at these temperatures. Optimization of all the data again was obtained using $k'_2 = 1.1 \times 10^9 e^{-24{,}000/RT}$ and $k'_3 = 5 \times 10^6 e^{-13{,}000/RT}$, and the fits are shown in Figs. 8b and 9b. The trends and curvature for N_2O are again provided by the inclusion of a reversible N_2O adsorption/desorption step. The parameter values for k and K_{CO} are also given in Table 5 for five temperatures. The k'_2 values in Table 5 typically agree within a factor of 2 with values measured independently for N_2O decomposition on La_2O_3 in the presence of H_2 or CO, with the exception of that at 773 K, which was around six times higher (12).

SUMMARY

In the absence of gas-phase O_2, the specific activity at 973 K for NO reduction to N_2 by H_2 over La_2O_3 is an order of magnitude higher than that for reduction by CH_4; however, a comparable amount of N_2O is also produced. With CO and no O_2, the specific activity is more than 4-fold higher than that with CH_4 but again large amounts of N_2O are formed. At 773 K, the NO conversion rate with H_2 is still 10-fold higher than that with CH_4, but the selectivity to N_2 is only about 20%, whereas with CO at this temperature, the activity for NO conversion is still about 4-fold higher compared with CH_4, but the selectivity to N_2 is only around 10% (90% N_2O). The addition of 1% O_2 to the feed reduces NO reduction rates significantly. This is due to the high combustion rates of H_2 and CO, at least in part; thus these two reductants are not selective in the presence of excess O_2. Very linear Arrhenius plots were obtained for N_2 formation with either reductant; in contrast, the N_2O plots exhibited pronounced bend-over at higher temperatures. Reaction models are proposed for each reaction that incorporate a reversible N_2O adsorption/desorption step into the sequence for N_2 formation. These models fit the Arrhenius and partial pressure dependency data well and can account for the observed trends over the entire temperature range.

ACKNOWLEDGMENT

This study was sponsored by the National Science Foundation under Grants CTS-9211552 and CTS-9633752.

REFERENCES

1. Armor, J. N., *Appl. Catal. B* **1**, 221 (1992).
2. Zhang, X., Walters, A. B., and Vannice, M. A., *Appl. Catal. B* **4**, 237 (1994).
3. Zhang, X., Walters, A. B., and Vannice, M. A., *J. Catal.* **155**, 290 (1995).
4. Zhang, X., Walters, A. B., and Vannice, M. A., *Catal. Today* **27**, 47 (1995).
5. Zhang, X., Walters, A. B., and Vannice, M. A., *Appl. Catal. B* **7**, 321 (1996).
6. Iizuka, T., Ikeda, H., Terao, T., and Tanabe, K., *Aust. J. Chem.* **35**, 927 (1982).
7. Shelef, M., and Gandhi, H. S., *Ind. Eng. Chem. Prod. Res. Dev.* **11**, 2 (1972).
8. Mochida, I., Suetsugu, K., Fujitsu, H., Takeshita, K., Tsuji, K., Sagara, Y., and Onyoshi, A., *J. Catal.* **77**, 519 (1982).
9. Lindstedt, A., Strömberg, D., and Milh, M. A., *Appl. Catal. A* **116**, 109 (1994).
10. Mizuno, N., Tanaka, M., and Misono, M., *J. Chem. Soc. Faraday Trans.* **88**, 91 (1992).
11. Viswanathan, B., *Catal. Rev. Sci. Eng.* **34**, 337 (1992).
12. Huang, S.-J., M.S. thesis, Pennsylvania State University, 1996.
13. Zhang, X., Walters, A. B., and Vannice, M. A., *J. Catal.* **146**, 568 (1994).
14. Huang, S.-J., Walters, A. B., and Vannice, M. A., *Appl. Catal. B*, in press.
15. Huang, S.-J., Ph.D. thesis, Pennsylvania State University, in progress.
16. Gschneidner, K. A., and Eyring, L., "Handbook on the Physics and Chemistry of Rare Earths." Vol. 5, North-Holland, Amsterdam, 1982.
17. Miller, J. A., and Bowman, C. T., *Prog. Energy Combust. Sci.* **15**, 287 (1989).
18. Boudart, M., and Djega-Mariadassou, G., "Kinetics of Heterogeneous Catalytic Reactions." Princeton Univ. Press, Princeton, NJ, 1984.
19. Yamashita, T., and Vannice, M. A., *J. Catal.* **161**, 254 (1996).
20. Rheaume, L., and Parravano, G., *J. Phys. Chem.* **63**, 264 (1959).
21. Boudart, M., Mears, D. E., and Vannice, M. A., *Ind. Chem. Belg.* **32**, 281 (1967).
22. Vannice, M. A., Hyun, S. H., Kalpacki, B., and Liauh, W. C., *J. Catal.* **56**, 358 (1979).